Journal of Fluorine Chemistry 132 (2011) 5–8

Contents lists available at ScienceDirect

Journal of Fluorine Chemistry

journal homepage: www.elsevier.com/locate/fluor

Temperature-dependent six-photon upconversion fluorescence of Er^{3+}

Kezhi Zheng, Dan Zhao, Daisheng Zhang, Ning Liu, Weiping Qin *

State Key Laboratory on Integrated Optoelectronics, College of Electronic Science and Engineering, Jilin University, Changchun 130012, China

ARTICLE INFO

Article history:
Received 23 August 2010
Received in revised form 7 October 2010
Accepted 22 October 2010
Available online 29 October 2010

Keywords:
Lanthanide ions
Temperature-dependent
Upconversion luminescence

ABSTRACT

Yb^{3+}/Er^{3+} codoped β-$NaYF_4$ microcrystals were synthesized through a facile EDTA-assisted hydrothermal method. Under 980 nm excitation, 244, 256, and 276 nm upconversion (UC) emissions were observed in $NaYF_4$:Yb^{3+}/Er^{3+} microcrystals, which were assigned to the $^2I_{11/2} \rightarrow {}^4I_{15/2}$, $^4D_{7/2} \rightarrow {}^4I_{15/2}$, and $^4G_{9/2} \rightarrow {}^4I_{15/2}$ transitions of Er^{3+} ions, respectively. Successive energy transfers (ETs) from Yb^{3+} to Er^{3+} played crucial roles in populating the high-energy states of Er^{3+} ions. Power dependence analysis exhibited that 244 and 256 nm UC emissions came from six-photon processes. Temperature-dependent UC emissions of $^4D_{7/2} \rightarrow {}^4I_{15/2}$ and $^2I_{11/2} \rightarrow {}^4I_{15/2}$ transitions of Er^{3+} were discussed and the nonradiative relaxation (NR) process of $^2I_{11/2} \rightarrow {}^4D_{7/2}$ was confirmed.

1. Introduction

During the past decades, short-wavelength solid-state lasers became research focus due to their widely applications, such as high density optical data storage, infrared (IR) sensors, color displays, and so on [1–3]. High-order frequency UC luminescence (UCL) based on trivalent lanthanide ions (Ln^{3+}) doped nano- and micro-crystals is particularly attractive in the past few years due to it could provide an available method to produce the short-wavelength lasers [4,5]. Er^{3+} ion is an ideal candidate for UCL since its intermediate levels ($^4I_{9/2}$, $^4I_{11/2}$, and $^4I_{13/2}$) can be conveniently populated by commercial low-cost near-infrared (NIR) and IR diode lasers. Up to now, UC studies of Er^{3+} doped materials have mainly focused on the visible region, which result in the development of UC solid-state lasers in visible region in Er^{3+} doped CaF_2, $LiYF_4$ (YLF), $Y_3Al_5O_{12}$ (YAG), $YAlO_3$ (YAP) and fluorozirconate fibers (ZBLAN) [6–10]. Ultraviolet (UV) and violet UC solid-state lasers are the next goals. As we all know, the biggest obstacle to develop the short-wavelength solid-state laser is synthesizing materials with efficient and intense short-wavelength emissions. Consequently, synthesizing the high-efficiency UV UCL materials and elucidating the UC mechanisms are the most important task for researchers today.

On the other hand, several factors, such as particle size, Ln^{3+} concentration, temperature, and pump power, have great effect on the UCL properties of Ln^{3+} ions [11–14]. Er^{3+} has close intermediate excited states, therefore, the nonradiative relaxation (NR) processes, which are associate with phonon density and sensitive to temperature, can occur inevitably in the UC process before Er^{3+} reach to high-energy states, leading to the UC emissions from neighbor levels of Er^{3+} present strong temperature- and power-dependent properties. Consequently, by changing pumping power and temperature, we can control some NR processes during the UC population, and it is a possible way to deeply understand the complex UC mechanism in Ln^{3+} doped luminescence materials. In addition, compared with oxides, hydroxides, and chlorides, fluorides with good stability and low phonon energy are considered as more suitable host materials for investigating UCL. The former made them possible as host materials to investigate the UCL, the latter would decrease the nonradiative relaxation process during the UC population and improve the short-wavelength UCL greatly. We surmised that β-$NaYF_4$, with a high refractive index and low phonon energy, would benefit for obtaining the high-order UCL of Er^{3+} ions [15].

In this paper, we presented an observation of temperature-dependent high-order UC emissions of Er^{3+} ions in Yb^{3+}–Er^{3+} codoped β-$NaYF_4$ microcrystals. Under 980 nm excitation, 244, 256, and 276 nm UC emissions of Er^{3+} were observed and assigned to the five- and six-photon UC processes. In the microcrystals, successive ETs from Yb^{3+} to Er^{3+} played important roles in populating the high-energy states of Er^{3+} ions. The temperature-dependent UC emission intensity ratio of $^4D_{7/2} \rightarrow {}^4I_{15/2}$ to $^2I_{11/2} \rightarrow {}^4I_{15/2}$ was discussed, which confirm the

* Corresponding author at: State Key Laboratory on Integrated Optoelectronics, College of Electronic Science and Engineering, Jilin University, 2699 Qianjin Street, Changchun 130012, China.
Tel.: +86 431 85168240 8325; fax: +86 431 85168240 8325.
E-mail address: wpqin@jlu.edu.cn (W. Qin).

0022-1139/$ – see front matter © 2010 Elsevier B.V. All rights reserved.
doi:10.1016/j.jfluchem.2010.10.003

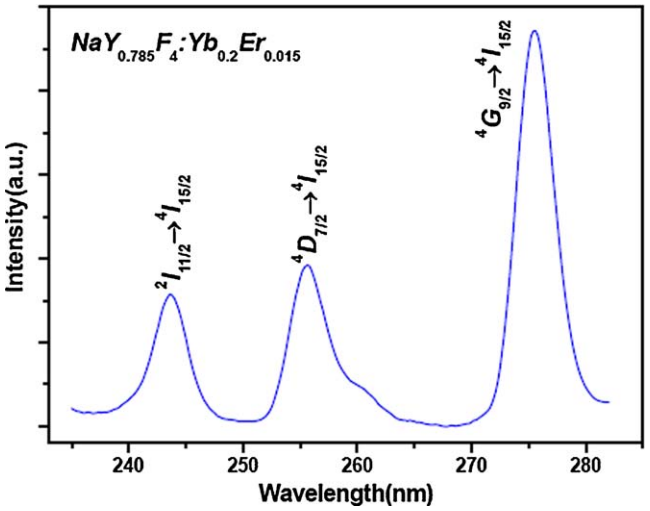

Fig. 1. UC luminescence spectrum of $NaYF_4$:Yb^{3+}/Er^{3+} microcrystals in the range of 235–282 nm.

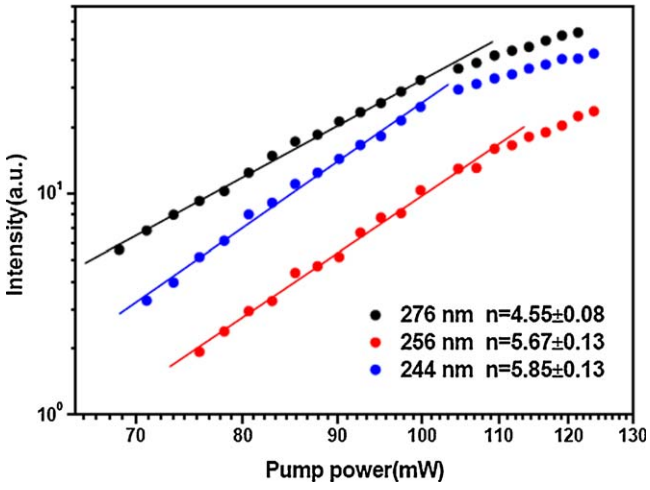

Fig. 3. Plots (log–log) of emission intensity versus excitation power in $NaYF_4$: Yb^{3+}/Er^{3+} microcrystals.

specific population process of high-energy excited states of Er^{3+} in this codoped sample.

2. Results and discussion

X-ray powder diffraction (XRD) analysis confirmed that the sample was hexagonal phase $NaYF_4$, which is in good agreement with the standard values for the β-$NaYF_4$ (JCPDS No. 16-0334). The corresponding morphology of the microcrystals is hexagonal prisms with uniform size distribution. Their diameters are 2–3 μm and lengths are 5 μm on average. At 980 nm excitation of ~300 mW, the annealed $NaYF_4$:20% Yb^{3+} and 1.5% Er^{3+} microcrystals emitted UV UC fluorescence, as shown in Fig. 1. Three peaks in the range of 235–282 nm were observed clearly. Emissions that peaked at 276, 256, and 244 nm originated from the $^4G_{9/2} \rightarrow {}^4I_{15/2}$, $^4D_{7/2} \rightarrow {}^4I_{15/2}$, and $^2I_{11/2} \rightarrow {}^4I_{15/2}$ transitions of Er^{3+}, respectively.

In Yb^{3+}–Er^{3+} codoped systems, different processes may result in upconversion. Fig. 2 describes schematically possible upconverted processes in energy level diagrams of Yb^{3+} and Er^{3+} ions [16]. In Yb^{3+}–Er^{3+} codoped β-$NaYF_4$ microcrystals, there exist two different UC routes to populate the intermediate states $^2H_{11/2}/{}^4S_{3/2}$ of Er^{3+} ions as follows: route 1: $^4I_{15/2} \xrightarrow{ET} {}^4I_{11/2} \xrightarrow{ET} {}^4F_{7/2} \xrightarrow{NR} {}^2H_{11/2}, {}^4S_{3/2}$; route 2: $^4I_{15/2} \xrightarrow{ET} {}^4I_{11/2} \xrightarrow{NR} {}^4I_{13/2} \xrightarrow{ET} {}^4F_{9/2} \xrightarrow{ET} {}^2H_{9/2} \xrightarrow{NR} {}^2H_{11/2}, {}^4S_{3/2}$

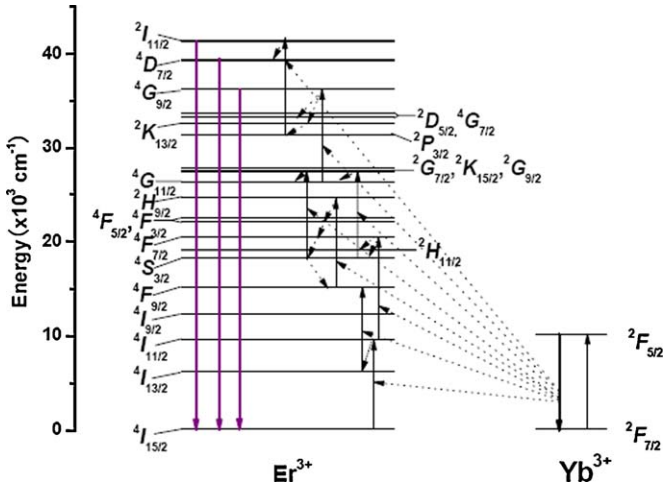

Fig. 2. Energy level diagrams of Yb^{3+} and Er^{3+} ions, and possible UC processes.

[17]. On the other hand, owing to the appropriate energy matching, the population processes from intermediate states $^2H_{11/2}/{}^4S_{3/2}$ to high-energy states $^4G_{9/2}$, $^4D_{7/2}$, and $^2I_{11/2}$ of Er^{3+} are the same in these two routes, which are depicted empirically in Fig. 2 as follow: $^2H_{11/2}/{}^4S_{3/2} \xrightarrow{ET} {}^2G_{7/2} \xrightarrow{NR} {}^4G_{11/2} \xrightarrow{ET} {}^4G_{9/2} \xrightarrow{NR} {}^4G_{7/2}, {}^2K_{13/2}, {}^2P_{3/2} \xrightarrow{ET} {}^2I_{11/2} \xrightarrow{NR} {}^4D_{7/2}$. The specific populate processes of high-energy states $^2I_{11/2}$ and $^4D_{7/2}$ of Er^{3+} ions in this codoped sample will be discussed in detail below. In the codoped β-$NaYF_4$ microcrystals, ET processes of $Yb^{3+} \rightarrow Er^{3+}$ operated continuously and effectively, which is benefit for populating the high-energy states of Er^{3+} ions and presenting their short-wavelength UC emissions effectively.

To understand the UC processes well, we investigated the excitation power I_{IR} dependence of UC fluorescence intensity I_f. For an unsaturated UC process, $I_f \propto I_{IR}^n$, where n is the number of the IR photons absorbed per upconverted photon emitted. Fig. 3 shows the double logarithmic plots of the emission intensity I_f as a function of excitation power I_{IR}. For the sample $NaY_{0.785}F_4$:$Yb_{0.2}Er_{0.015}$ and under 980 nm excitation, the obtained n were 4.55 ± 0.08, 5.67 ± 0.13, and 5.85 ± 0.13 for the emissions of 276,

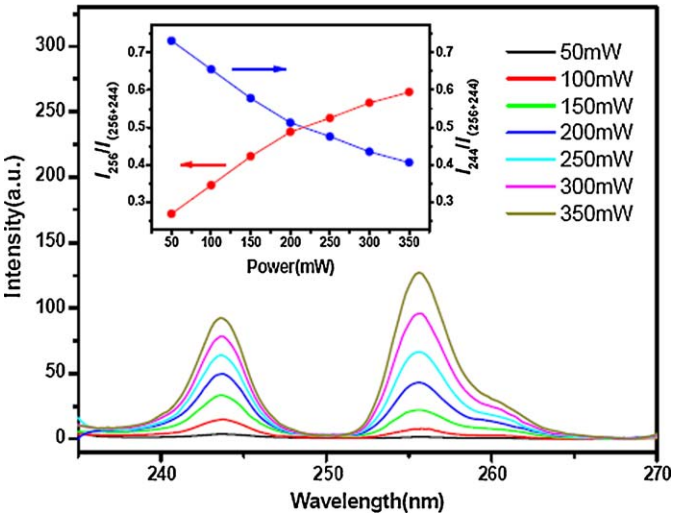

Fig. 4. Excitation power dependence of UC emission spectra of $NaYF_4$:20% Yb^{3+}, 1.5% Er^{3+} microcrystals. The inset is the ratios of 244 nm emission intensity I_{244} and 256 nm emission intensity I_{256} to the total integrated intensity $I_{(256+244)}$ in the range of 235–270 nm, respectively.

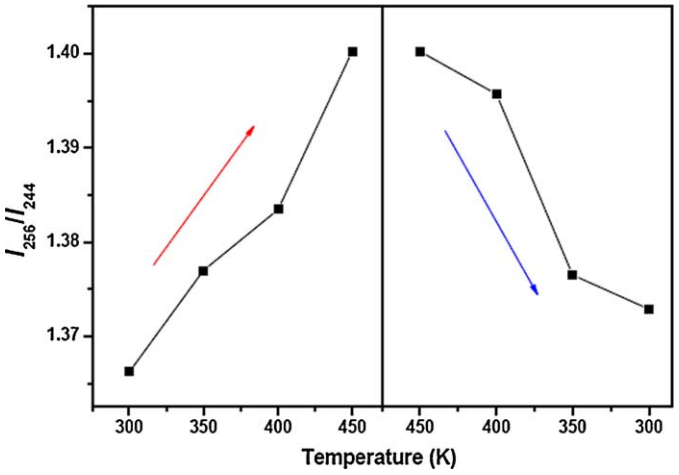

Fig. 5. Intensity ratio of $^4D_{7/2} \rightarrow {}^4I_{15/2}$ (I_{256}) to $^2I_{11/2} \rightarrow {}^4I_{15/2}$ (I_{244}) as a function of temperature. Rising process: 300–450 K; falling process: 450–300 K.

256, and 244 nm, respectively, which indicated that the $^4G_{9/2} \rightarrow {}^4I_{15/2}$, $^4D_{7/2} \rightarrow {}^4I_{15/2}$, and $^2I_{11/2} \rightarrow {}^4I_{15/2}$ transitions of Er^{3+} came from five-, six-, and six-photon UC process, respectively. These results accord well with the possible UC processes we proposed in Fig. 2. Additionally, to the best of our knowledge, six-photon UC processes of Er^{3+} ions under NIR excitation have not been observed before. Compared with the high-order UC processes we observed in Yb^{3+}–Tm^{3+} codoped systems, these multiphoton UC processes in Yb^{3+}–Er^{3+} codoped systems are more difficult to obtain, owing to the reasons as described below. Firstly, Er^{3+} has ladder-like medial excited-state manifolds, which lead to excited Er^{3+} ions losing energy radiatively or nonradiatively before they reach to higher states. Secondly, the inevitable back energy transfer from excited Er^{3+} to adjacent Yb^{3+} ions also oppresses the progress of high-order UC.

Fig. 4 is the excitation power dependence of UC emission spectra of the sample. It is obviously that the relative intensity of 244 and 256 nm UC emissions changed by varying the excitation power. At pump power lower than 200 mW, the emission intensity of 256 nm is lower than that of 244 nm, and it becomes the dominance between these two emissions while the excitation power increases to the region of 200–350 mW. The inset of Fig. 4 shows the integrated emission intensity ratios of I_{256} and I_{244} to the

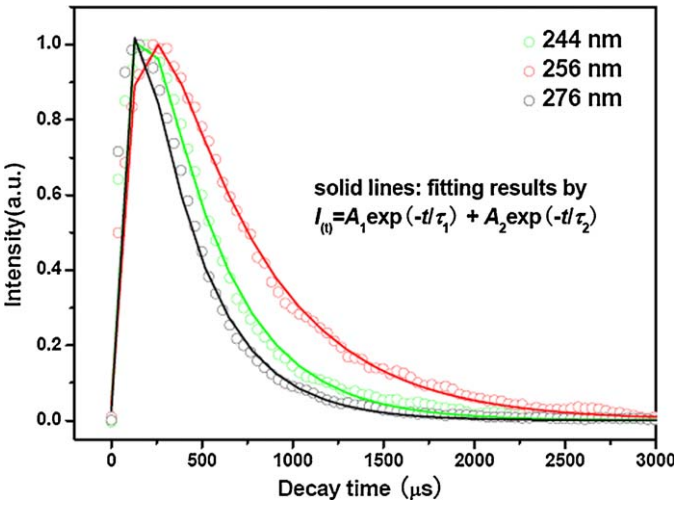

Fig. 6. The time-dependent emission curves of Er^{3+} (λ_{ex} = 953.6 nm, λ_{em} = 244, 256, and 276 nm represent the $^2I_{11/2} \rightarrow {}^4I_{15/2}$, $^4D_{7/2} \rightarrow {}^4I_{15/2}$, and $^4G_{9/2} \rightarrow {}^4I_{15/2}$ transitions of Er^{3+}, respectively) in $NaYF_4$:20% Yb^{3+}/1.5% Er^{3+} microcrystals. Open circles: experimental data; solid lines: fitting results by $I_{(t)} = A_1 \exp(-t/\tau_1) + A_2 \exp(-t/\tau_2)$.

Table 1
The rise time τ_1 and decay time τ_2 for 244, 256, and 276 nm UC emissions of Er^{3+} calculated from the time-dependent emission profiles.

	244 nm	256 nm	276 nm
Rise time τ_1 (μs)	93.7	121	69.6
Decay time τ_2 (μs)	383	555	329.8

total integrated intensity $I_{(256+244)}$ in the range of 235–270 nm, indicating that I_{256} increases with increasing the excitation power while I_{244} decreases. As described above, 256 and 244 nm UC emissions came from the $^4D_{7/2} \rightarrow {}^4I_{15/2}$ and $^2I_{11/2} \rightarrow {}^4I_{15/2}$ transitions of Er^{3+}, respectively, and NR process of $^2I_{11/2} \rightarrow {}^4D_{7/2}$ was empirically proposed between these two states. As we all know, the rate of multiphonon relaxation is dominated by $(1 + \langle n \rangle)^P$, where n is the phonon density

$$\left(\langle n \rangle = \frac{1}{1 - \exp(-\hbar\omega/K_B T)}\right)$$

and

$$P = \frac{-\Delta E}{\hbar\omega}.$$

$\hbar\omega$, K_B, T, and ΔE represent phonon energy, Boltzmann constant, temperature, and energy gap, respectively. The higher T is, the larger rate of multiphonon relaxation is. Under 980 nm NIR excitation, some of NIR light energy inevitably transfers to thermal energy, leading to the increase of temperature in the irradiated region. The higher excitation power is, the higher T is. Therefore, the multiphonon relaxation rate of $^2I_{11/2} \rightarrow {}^4D_{7/2}$ increases with the increase of excitation power, which makes the variation of relative emission intensity ratio ($I_{256}/I_{(256+244)}$ and $I_{244}/I_{(256+244)}$), as depicted in Fig. 4, to be understood clearly.

To further elucidate the temperature dependence of UC emissions of 256 and 244 nm, we investigated the relative intensity ratio of I_{256}/I_{244} at different temperatures and under 980 nm excitation at ~300 mW. The relative intensity ratio of $^4D_{7/2} \rightarrow {}^4I_{15/2}$ to $^2I_{11/2} \rightarrow {}^4I_{15/2}$ transitions as a function of temperature is shown in Fig. 5. It is interesting to see that I_{256}/I_{244} increases with increasing the temperature, and decreases with a decrease of temperature. The experimental results further confirm the multiphonon relaxation process between $^2I_{11/2}$ and $^4D_{7/2}$ states, which has been well explained above. Therefore, we conclude that for populating the high-energy state $^4D_{7/2}$ of Er^{3+} ions in the Yb^{3+}–Er^{3+} codoped sample, the direct ET processes from Yb^{3+} to Er^{3+} occurred with less possibility owing to the inappropriate energy matching, and the dominant populate process for the excited $^4D_{7/2}$ under 980 nm excitation is $^2P_{3/2} \xrightarrow{ET} {}^2I_{11/2} \xrightarrow{NR} {}^4D_{7/2}$, as depicted in Fig. 2.

The time resolved fluorescence intensity of $^4G_{9/2}$, $^4D_{7/2}$, and $^2I_{11/2}$ levels of Er^{3+} ions has also been measured in Yb^{3+}–Er^{3+} codoped β-$NaYF_4$ microcrystals, as shown in Fig. 6. These decay curves can be fitted well into double-exponential function as $I_{(t)} = A_1 \exp(-t/\tau_1) + A_2 \exp(-t/\tau_2)$ with a short rise time τ_1 and a long decay time τ_2. They show rise time before they start decaying, which provide powerful evidence of the ETs from Yb^{3+} to Er^{3+}. There are two time constants in the best-fitted results, as shown in Table 1. The long one, τ_2 = 329.8, 555, and 383 μs, is the lifetime of $^4G_{9/2}$, $^4D_{7/2}$, and $^2I_{11/2}$ levels, respectively.

3. Conclusions

In conclusion, under 980 nm excitation, UV UC fluorescence of Er^{3+} ions was observed in Yb^{3+}–Er^{3+} codoped β-$NaYF_4$

microcrystals, which were synthesized successfully through a facile EDTA-assisted hydrothermal method. 276, 256, and 244 nm UC emissions were observed and assigned to the $^4G_{9/2} \rightarrow {}^4I_{15/2}$, $^4D_{7/2} \rightarrow {}^4I_{15/2}$, and $^2I_{11/2} \rightarrow {}^4I_{15/2}$ transitions of Er^{3+}, respectively. Power dependent analysis confirmed that 256 and 244 nm UC emissions of Er^{3+} ions came from six-phonon processes. In the codoped sample, successive ETs from Yb^{3+} to Er^{3+} play crucial roles in populating the excited Er^{3+} and producing the high-order UC emissions of Er^{3+} ions. The relative emission intensity ratio of 256–244 nm UC emissions of Er^{3+} exhibited temperature dependent characteristic, which is attributed to the multiphonon relaxation process of $^2I_{11/2} \rightarrow {}^4D_{7/2}$. The synthetic β-$NaYF_4$:$Yb^{3+}$/$Er^{3+}$ microcrystals provide a possible candidate material for building UV compact solid-state lasers or fiber laser.

4. Experimental details

4.1. Sample preparation

Ethylene diamine tetraacetic acid (EDTA), NaF, and nitric acid (HNO_3) were supplied by Beijing Fine Chemical Company, and were of analytical grade. Yttrium oxide (Y_2O_3, 99.99%), ytterbia (Yb_2O_3, 99.999%), and erbium oxide (Er_2O_3, 99.999%) were supplied by Shanghai Shabo Chemical Reagent Company. All the chemicals were used as received without further purification. Y_2O_3, Yb_2O_3, and Er_2O_3 were dissolved in dilute HNO_3 by heating to prepare the stock solution of $Y(NO_3)_3$, $Yb(NO_3)_3$, and $Er(NO_3)_3$. In a typical synthesis of $NaYF_4$:20% Yb^{3+} and 1.5% Er^{3+}, 2 mmol $Ln(NO_3)_3$ (Ln = Y, Yb, and Er) (0.5 M) was added to a separately prepared solution containing 2 mmol of EDTA (dissolved in 20 mL of H_2O). After stirring of the solution vigorously for 30 min, 32 mmol of NaF (dissolved in 20 mL of H_2O) was added and the stirring was continued for 30 min. Afterward, the mixture was sealed in two 50 mL Teflon-lined stainless steel autoclaves and maintained at 160 °C for 18 h. After the autoclaves were cooled down to room temperature naturally, the resulting precipitates were separated by centrifugation, washed with deionized water and ethanol several times, and then dried at 60 °C for 20 h. To improve the crystallinity of the microcrystalline powder, the sample was annealed in an argon atmosphere at 400 °C for 1.5 h.

4.2. Characterization

The crystal structure was analyzed by a Rigaku RU-200b X-ray powder diffractometer (XRD) using a nickel-filtered Cu-Kα radiation (λ = 1.5406 Å). The size and morphology were investigated by scanning electron microscope (SEM, Hitachi TM-1000). All the UCL spectra were recorded using a Hitachi F-4500 fluorescence spectrophotometer which equipped with a 980 nm CW diode laser and detected by R928 (Hamamatsu) (2.5 nm for slit width and 400 V for PMT voltage). In the measurements of temperature-dependent UCL, a set of home-made equipment was used to control the sample temperature. The temporal property was studied using a 953.6 nm Raman shifter laser (pumped by the second harmonic of a Nd:YAG pulsed laser, pulse width 10 ns, repetition rate 10 Hz) and an oscillograph.

Acknowledgments

This work was supported by the National High Technology Research and Development Program of China (863 Program: 2009AA03Z309) and the National Natural Science Foundation of China (NNSFC) (grants 10874058 and 60908031).

References

[1] F. Auzel, Chem. Rev. 104 (2004) 139–174.
[2] T. Hebert, R. Wannemacher, W. Lenth, R. Macfarlane, Appl. Phys. Lett. 57 (1990) 1727–1729.
[3] Y. Mita, K. Hirama, N. Ando, H. Yamamoto, S. Shionoya, J. Appl. Phys. 74 (1993) 4703.
[4] W. Qin, C. Cao, L. Wang, J. Zhang, D. Zhang, K. Zheng, Y. Wang, G. Wei, G. Wang, P. Zhu, Opt. Lett. 33 (2008) 2167–2169.
[5] G. Wang, W. Qin, L. Wang, G. Wei, P. Zhu, R. Kim, Opt. Express 16 (2008) 11907–11914.
[6] S. Pollack, D. Chang, N. Moise, J. Appl. Phys. 60 (1986) 4077.
[7] P. Xie, S. Rand, Opt. Lett. 17 (1992) 1198–1200.
[8] J. Kliava, A. Malakhovskii, I. Edelman, A. Potseluyko, E. Petrakovskaja, I. Bruckental, Y. Yeshurun, T. Zarubina, J. Supercond. Nov. Magn. 20 (2007) 149–153.
[9] A. Silversmith, W. Lenth, R. Macfarlane, Appl. Phys. Lett. 51 (1987) 1977–1979.
[10] S. Georgescu, O. Toma, SPIE 5581 (2004) 245.
[11] H. Song, B. Sun, T. Wang, S. Lu, L. Yang, B. Chen, X. Wang, X. Kong, Solid State Commun. 132 (2004) 409–413.
[12] H. Guo, N. Dong, M. Yin, W.P. Zhang, L.R. Lou, S.D. Xia, J. Phys. Chem. B 108 (2004) 19205–19209.
[13] X. Bai, H. Song, G. Pan, Y. Lei, T. Wang, X. Ren, S. Lu, B. Dong, Q. Dai, L. Fan, J. Phys. Chem. C 111 (2007) 13611–13617.
[14] Y. Wang, L.P. Tu, J.W. Zhao, Y.J. Sun, X.G. Kong, H. Zhang, J. Phys. Chem. C 113 (2009) 7164–7169.
[15] K.W. Krämer, D. Biner, G. Free, H.U. Güdel, M.P. Hehlen, S.R. Lüthi, Chem. Mater. 16 (2004) 1244–1251.
[16] W.T. Carnall, P.R. Fields, K. Rajnak, J. Chem. Phys. 49 (1968) 4424–4442.
[17] K. Zheng, L. Wang, D. Zhang, D. Zhao, W. Qin, Opt. Express 18 (2010) 2934–2939.